Biodegradable nanofiber-based piezoelectric transducer

Eli J. Curry[a,1], Thinh T. Le[b,1], Ritopa Das[a], Kai Ke[c], Elise M. Santorella[d], Debayon Paul[d], Meysam T. Chorsi[b], Khanh T. M. Tran[a], Jeffrey Baroody[a], Emily R. Borges[a], Brian Ko[e], Asiyeh Golabchi[f], Xiaonan Xin[g], David Rowe[g], Lixia Yue[h], Jianlin Feng[h], M. Daniela Morales-Acosta[i], Qian Wu[j], I-Ping Chen[k], X. Tracy Cui[f], Joel Pachter[d], and Thanh D. Nguyen[a,b,i,2]

[a]Department of Biomedical Engineering, University of Connecticut, Storrs, CT 06269; [b]Department of Mechanical Engineering, University of Connecticut, Storrs, CT 06269; [c]College of Polymer Science and Engineering, Sichuan University, Chengdu 610065, Sichuan, China; [d]Blood–Brain Barrier Laboratory, Department of Immunology, University of Connecticut Health Center, Farmington, CT 06030; [e]Department of Agricultural and Biological Engineering, Mississippi State University, Mississippi State, MS 39762; [f]Department of Bioengineering, University of Pittsburgh, Pittsburgh, PA 15260; [g]Center for Regenerative Medicine and Skeletal Development, University of Connecticut Health Center, Farmington, CT 06030; [h]Department of Cell Biology, University of Connecticut Health Center, Farmington, CT 06030; [i]Institute of Materials Science, University of Connecticut, Storrs, CT 06269; [j]Pathology and Laboratory Medicine, University of Connecticut Health Center, Farmington, CT 06030; and [k]Department of Oral Health and Diagnostic Sciences, School of Dental Medicine, University of Connecticut Health Center, Farmington, CT 06030

Piezoelectric materials, a type of "smart" material that generates electricity while deforming and vice versa, have been used extensively for many important implantable medical devices such as sensors, transducers, and actuators. However, commonly utilized piezoelectric materials are either toxic or nondegradable. Thus, implanted devices employing these materials raise a significant concern in terms of safety issues and often require an invasive removal surgery, which can damage directly interfaced tissues/organs. Here, we present a strategy for materials processing, device assembly, and electronic integration to 1) create biodegradable and biocompatible piezoelectric PLLA [poly(L-lactic acid)] nanofibers with a highly controllable, efficient, and stable piezoelectric performance, and 2) demonstrate device applications of this nanomaterial, including a highly sensitive biodegradable pressure sensor for monitoring vital physiological pressures and a biodegradable ultrasonic transducer for blood–brain barrier opening that can be used to facilitate the delivery of drugs into the brain. These significant applications, which have not been achieved so far by conventional piezoelectric materials and bulk piezoelectric PLLA, demonstrate the PLLA nanofibers as a powerful material platform that offers a profound impact on various medical fields including drug delivery, tissue engineering, and implanted medical devices.

biodegradable | piezoelectric | PLLA | pressure sensors | ultrasound transducer

The ability to create biodegradable and biocompatible piezoelectric materials and small-scale devices (1, 2) could bring about significant biomedical applications, ranging from medical sensing (3), tissue engineering (4), and cellular manipulation (5), to controlled drug delivery (6).

Piezoelectric materials, a type of "smart" material that generates electricity while deforming and vice versa (1), are used in many important implantable medical devices such as sensors, transducers, and actuators. Piezoelectric sensors have been used along with medical catheters inside the body to monitor important physiological pressures such as intracranial pressure (7), blood pressure (8), bladder pressure (9), etc. More recently, researchers have developed implanted piezoelectric ultrasonic transducers to disrupt the blood–brain barrier (BBB) and facilitate the delivery of drugs into the brain (10). The BBB, which is composed of tight junctions between the endothelial cells in the blood vessels of the brain, prevents most therapeutics from accessing the brain tissue and thus is a major hurdle for the treatment of brain diseases (e.g., cancers). There are several established methods for opening the BBB, which include solvent, adjuvant, acoustic wave, lipidization, and osmostic pressure; ultrasound (US) or acoustic waves have

been extensively studied and shown to be safe and the most effective tool (11–13). However, the use of external US is limited to small animals with thin skull bones. Since the human skull is thick and absorbs more than 90% of US energy, it requires a large and bulky array of external US transducers, a complicated energy-focusing operation, and a tedious MRI (magnetic resonance imaging) monitoring procedure (11, 12). This extensive process would be useful for a single treatment like viral gene delivery-based approaches (14). However, in certain applications such as chemotherapy, research has shown the opening of the BBB requires repetitive treatment (15). As such, implanted US transducers (e.g., Sonocloud) have emerged as an excellent alternative, which can repeatedly induce low-intensity sonication deep inside brain tissue at a precise location to open the BBB without causing any damage to the surrounding brain tissue (10, 15). Unfortunately, all of the aforementioned pressure sensors and US transducers rely on conventional piezoelectric materials such as PZT (lead zirconate titanate), PVDF (polyvinylidene fluoride), ZnO (zinc oxide), etc., which are either toxic and/or nondegradable. Thus, these piezoelectric devices pose significant concerns regarding safety after

Significance

This paper describes a powerful biodegradable and biocompatible piezoelectric nanofiber platform for significant medical implant applications, including a highly sensitive, wireless, biodegradable force sensor for the monitoring of physiological pressures, and a biodegradable ultrasonic transducer for the delivery of drugs across the blood–brain barrier. Built upon materials commonly utilized in medical implants, the devices can self-degrade, causing no harm to the body, and avoid any invasive removal surgeries.

implantation and require a removal surgery, which is invasive and deleterious to directly interfaced organs or tissues.

PLLA [poly(L-lactic acid)], a biocompatible and biodegradable medical polymer (16–18), has been shown to exhibit piezoelectricity when appropriately processed, thereby offering an excellent platform to construct safer, biodegradable piezoelectric implants, which can avoid problematic removal surgeries (3, 19). Previously, our group has employed thermally stretched, compression-molded PLLA bulk films to create a biodegradable piezoelectric force sensor (3). However, stretched PLLA bulk films pose several problems, including low reproducibility, film rigidity, and modest piezoelectric constants (~5 to 12 pC/N) (20, 21), which render the bulk PLLA films useless for actuators, transducers or highly sensitive pressure sensors. Recently, biodegradable amino acid crystals (e.g., glycine) have been reported with an excellent piezoelectric constant (22). However, it is challenging to fabricate these powder-based materials into functional films and orient the crystals in a repeatable manner to obtain a controllable piezoelectric performance for device applications. A few researchers have utilized electrospinning to create flexible PLLA piezoelectric nanofiber films (23–25), but the reported works struggle with major limitations. First, these reports lack appropriate material processing to stabilize the nanomaterial or utilize the shear-piezoelectric mode (i.e., d_{14}) of PLLA for an optimal piezoelectric performance. Consequently, the PLLA nanofibers can only produce small, unstable electrical signals under applied force (23). Second, the measured electrical signals are often mixed with other noises caused by friction between the rough nanofiber film and metal electrodes, commonly known as the triboelectric effect (24). Third, there is no report on the ability to control the piezoelectric performance of the PLLA nanofibers. These major drawbacks collectively restrict applications of this nanomaterial. As a result, there are only a few reported applications of piezoelectric PLLA nanofibers for nondegradable and nonimplantable force sensors or energy harvesters.

Here, we present a strategy for materials processing, device assembly, and electronic integration to 1) achieve biodegradable and biocompatible piezoelectric PLLA nanofibers with a highly controllable, efficient, and stable piezoelectric performance, and 2) demonstrate biodegradable, safe piezoelectric devices built upon this powerful nanomaterial (Fig. 1). First, we show that a biodegradable force sensor, made with the PLLA nanofiber film, possesses higher sensitivity and flexibility than that of the reported thermally stretched PLLA bulk film (3) and can be used to wirelessly monitor vital physiological pressures. Second, we demonstrate the same PLLA nanofiber sensor acts as a biodegradable ultrasonic transducer that can be implanted into the brain to open the BBB and safely self-degrade, causing no harm to the body. Despite several achievements in the field of biodegradable electronics (26–30), this report introduces a biodegradable, highly efficient piezoelectric US transducer, which is only made of materials commonly utilized in medical implants to facilitate the BBB opening for the delivery of drugs into the brain.

In order to improve the piezoelectric response of PLLA, the two major material properties that need to be addressed are the crystallinity and orientation of the polymer chains. By improving these properties, the carbon–oxygen double bonds (C=O) present in the helical PLLA backbone become aligned resulting in an inherent net polarization, and a well-documented shear piezoelectric response under applied force (31, 32). The PLLA nanofibers are made using a custom electrospinning setup, as seen in *SI Appendix*, Fig. S1. The speed of the rotating drum was varied from 300 to 4,000 rpm, while other parameters such as the voltage applied to the needle, distance to collector, needle gauge, flow rate, and solution concentrations were held constant. This resulted in PLLA nanofiber mats with different levels of fiber orientation. The nanofiber samples initially made by the electrospinning setup are highly amorphous and unstable, as
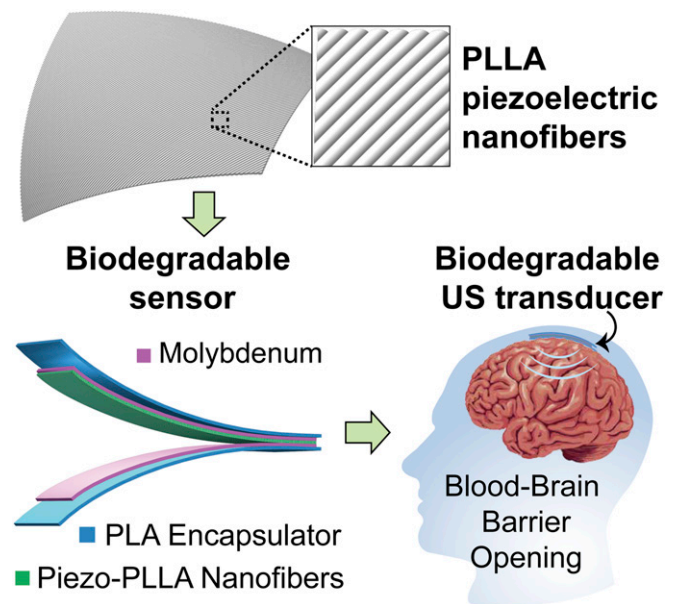

Fig. 1. PLLA nanofibers with highly controllable and excellent piezoelectric performance for biodegradable implanted piezoelectric devices. The image at *Top* is a simplified schematic of the treated piezoelectric PLLA nanofibers. The image at *Bottom Left* is the schematic of a biodegradable pressure sensor and ultrasound (US) transducer. The image at *Bottom Right* is a schematic illustrating the biodegradable US transducer, implanted inside the brain, which can repeatedly induce US to open the blood–brain barrier (BBB) and facilitate the delivery of drugs into the brain.

seen by the DSC (differential scanning calorimetry) (*SI Appendix*, Fig. S2). Therefore, the samples were carefully annealed and slowly cooled down in two serial steps at 105 and 160.1 °C to improve the crystallinity (*SI Appendix, Methods*). After these annealing processes, the crystallinities of the processed nanofiber samples appear to be in about the same range of 70 to 88% (see DSC data of Fig. 2*A*). The nanofiber films, collected at smaller spin speeds, have lower levels of fiber alignment. Therefore, we chose the 300 rpm electrospun PLLA sample as a negative control due to its lower crystallinity and poor fiber orientation (*SI Appendix*, Fig. S3), which results in little-to-no piezoelectric effect. XRD (X-ray diffraction) data in *SI Appendix*, Fig. S4, show that all of the samples are predominantly (200) and (110) crystal phases, indicating the presence of β-form crystal structures (33), which is the piezoelectric phase of PLLA (3). Additionally, as seen in the 2D XRD images of Fig. 2*B* and *SI Appendix*, Fig. S3*B*, electrospinning with a faster collector speed improves the orientation of the crystal domains in each nanofiber. The fiber alignment over the entire film also appeared to increase with faster collector speeds, as seen in the scanning electron microscopy (SEM) images (Fig. 2*C* and *SI Appendix*, Fig. S3*C*). However, macroscopic orientation of the PLLA fibers and the molecular alignment are also related to the jet speed (dictated by applied voltage used for electrospinning) (*SI Appendix*, Fig. S5). By tuning the jet speed to match the drum speed, the optimal piezoelectric PLLA film can be generated. Estimation of the crystallinity (using DSC) and Herman's orientation factor (using 2D XRD) for the electrospun PLLA samples is described in Fig. 2*D*, which shows that improving the collector drum speed generally results in higher crystallinity and crystal alignment in the nanofibers. Thus, by tailoring the collector and jet speeds, we can control the piezoelectricity of the nanofibers.

We then assessed the piezoelectric performance of the PLLA nanofiber films through an impact test (i.e., generation of voltage
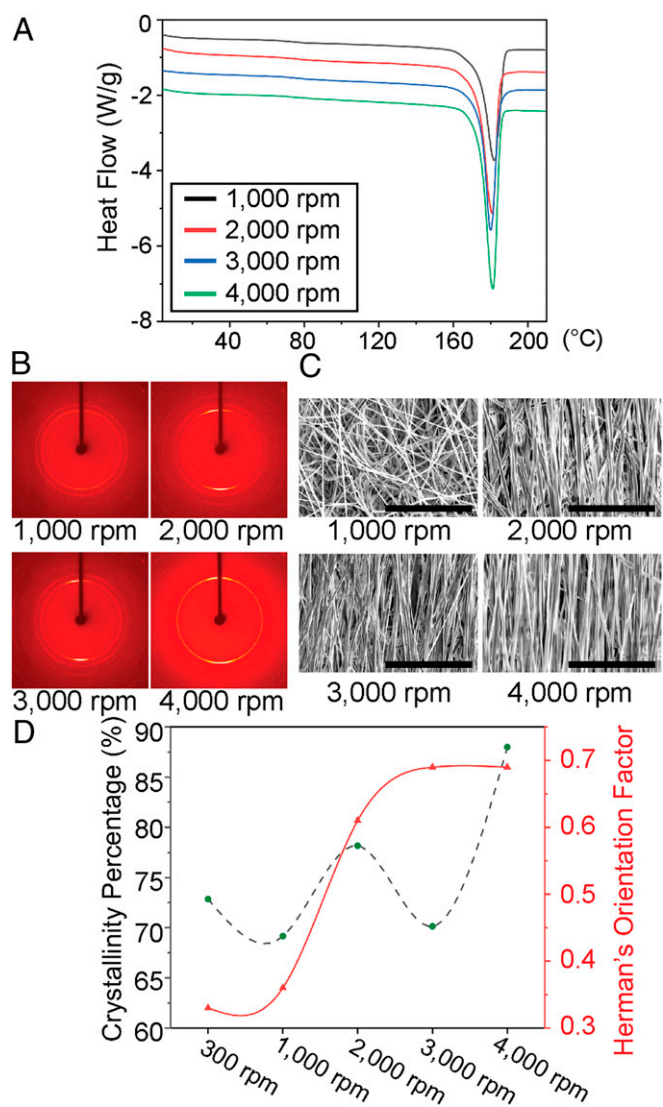
Curry et al.

Fig. 2. Material characterization of the electrospun PLLA. (*A*) Results from differential scanning calorimetry (DSC) of electrospun PLLA nanofiber films collected at different spin speeds. (*B*) The 2D X-ray diffraction (2D XRD) images show orientation of crystal domains inside the electrospun PLLA nanofibers, made with different collection speeds. (*C*) Scanning electron microscopy (SEM) images show PLLA nanofiber alignment with different collection speeds. (Scale bars, 40 μm.) (*D*) Graphical summary illustrating the trend that, as the PLLA nanofibers are collected at faster speeds, the Herman orientation factor (i.e., crystal alignment) and crystallinity percentage generally increase.

under impact force) and an actuation test (i.e., displacement under an applied electric field) (3, 20). To create the PLLA sensor for these tests, we fully annealed and cut the PLLA film at a 45° angle relative to the fiber direction to utilize shear piezo-electricity by maximizing shear force under an applied normal force. The fully treated and cut PLLA films possess a stable, efficient, and highly controllable piezoelectric performance, which has not been achieved by previous reports for the PLLA nanofibers (25, 32, 34). We then sandwiched the films between aluminum foil electrodes and Kapton tape (*SI Appendix, Methods*). For impact testing, the PLLA sensor is subjected to a consistent force induced by an actuator, which is integrated with a dynamic force sensor and driven by a defined voltage waveform. The charge output from the PLLA sample is measured with an electrometer (*SI Appendix, Methods*). All of the sensors

have the same area of 161.29 mm^2 and thicknesses in the range of 19 to 28 μm (*SI Appendix, Methods*). Additionally, prior to fabrication of the sensors, all of the films are soaked in deionized water to minimize the influence of the triboelectric effect (35). Fig. 3*A* illustrates charge outputs from the PLLA samples subjected to a 30-N impact force. The signals generated from the 6 treated PLLA samples clearly show the electrospun sample collected at 4,000 rpm has the largest charge output of about 0.9 nC while the 300 rpm sample exhibits little-to no charge output (~0.1 nC). The highly aligned nanofiber film, collected at 3,000 and 4,000 rpm drum speeds, noticeably outperforms the bulk pie-zoelectric PLLA film [annealed and stretched with a 3.5 draw ratio (DR), following our previous report (3)]. All open-circuit voltage outputs for these piezoelectric nanofiber films were reversible when the electrode connections were swapped (*SI Appendix,* Fig. S6), indicating that the PLLA is truly polarized, and that the measured signal is minimally influenced by tri-boelectricity. The impact measurement was also repeated using dry films, and the resulting data was used to estimate the shear piezoelectric coefficient (d$_{14}$) for all of the samples (*SI Appendix,* Fig. S7). Using the measured mechanical properties of the PLLA films (*SI Appendix,* Fig. S7*A*), we can roughly estimate the piezo-electric constant of the samples, based on our previously reported model (3); the 4,000 rpm sample appears to exhibit a d$_{14}$ of ~19 pC/N, while the conventional bulk PLLA film only exhibits a d$_{14}$ of ~12 pC/N (*SI Appendix,* Fig. S7*B*). This indicates the processing of PLLA nanofibers significantly improves the material's shear pie-zoelectric response. Furthermore, our strategy of cutting the PLLA films at 45° angles to utilize shear piezoelectricity was also justified by comparing the charge outputs of a 0° and 45° cut film under the same applied force (*SI Appendix,* Fig. S8). For the actuation mea-surement, a treated PLLA film (1.27 cm × 1.27 cm) was sandwiched in the center of aluminum foil electrodes (9.53 mm × 9.53 mm). A controlled voltage waveform was then applied to the sensor, and the displacement in the exposed right corner of the sample was mea-sured using a laser displacement sensor (*SI Appendix, Methods*). As seen in Fig. 3*B*, the treated PLLA nanofiber samples vibrate with the same frequency (1 Hz) as the applied sinusoidal voltage wave-form (20 V$_{pp}$). The 4,000 rpm electrospun sample again exhibits the greatest displacement (~4.5 μm), while the stretched 3.5 DR bulk film and 300 rpm electrospun samples exhibited no measurable displacement. This result confirms the superior piezoelectric performance of the highly aligned nanofiber film. In ad-dition, as the amplitude of the applied voltage increases, the amplitude of displacement for the electrospun films also increases, and the displacement is frequency dependent (Fig. 3*C* and *SI Appendix,* Fig. S9). Piezoelectric performance in the treated PLLA nanofiber film is also stable. This advantage is significant as there has been little research to avoid depolarization of the PLLA nanofibers over time (25, 32, 34). Indeed, as seen in Fig. 3*D*, only an elec-trospun sample (3,000 rpm) that underwent our full annealing processes (i.e., annealed at both 105 and 160.1 °C) has a stable piezoelectric output under the same applied force (~30 N) for 7 d, with a marginal loss (~6%) in signal at 14 d. In contrast, the untreated (i.e., not annealed) and partially treated (i.e., annealed only at 105 °C) samples rapidly lose their performance and are therefore not stable for long-term implant applications.

After verifying the piezoelectric effect of the PLLA nano-fibers, we create a biodegradable force sensor by using the nanofibers, molybdenum (Mo) electrodes, and encapsulating untreated PLLA layers (Fig. 1). PLLA or PLA are common biodegradable polymers used in Food and Drug Administration (FDA)-approved implanted tissue scaffolds, bone screws, and drug carriers (36). Molybdenum is a common nutrient (37) and a biodegradable metal, used extensively in FDA-approved hip and joint implants (38). Although we previously reported on a bio-degradable piezoelectric force sensor, the device is based on the stretched PLLA bulk film, which is less flexible, exhibits much
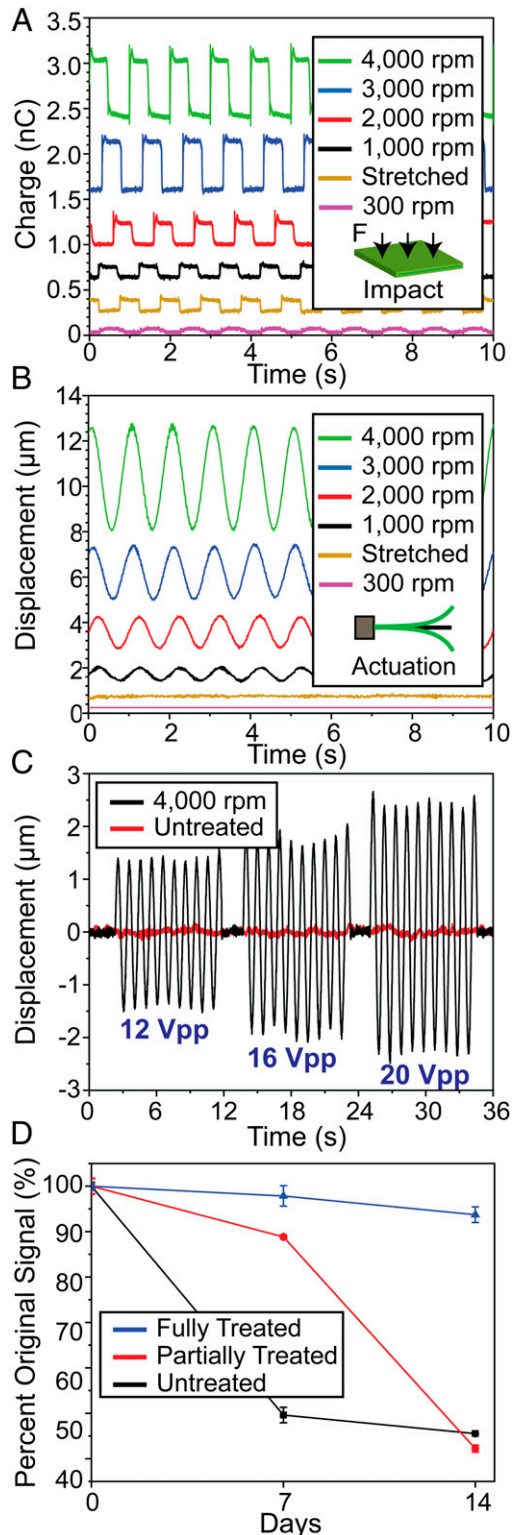
Curry et al.

www.manaraa.com

Fig. 3. Piezoelectric characterization of the treated PLLA nanofiber films. (*A*) Charge output from stretched, bulk piezo-PLLA (yellow) and treated electrospun PLLA, collected at different speeds, under the same impact force. (*B*) Displacement of stretched, bulk PLLA (yellow) and treated electrospun PLLA, collected at different speeds, under the same voltage (20 V$_{pp}$) at 1 Hz. (*C*) Displacement of 300 rpm PLLA negative-control sample (red) and 4,000 rpm PLLA (black), under increasing magnitudes of voltage at 1 Hz. (*D*) Comparison of the piezoelectric performance for 3,000 rpm electrospun PLLA samples annealed under different conditions over a 14-d period.

lower piezoelectric performance, and consequently offers lower sensitivity for force detection. Fig. 4*A* clearly illustrates this by showing that the slope of a calibration curve for a biodegradable sensor made with a treated 4,000 rpm electrospun PLLA film is 1.8 times steeper than that of a sensor, using a conventional thermally stretched, bulk PLLA film (DR = 3.5), reported in our previous work (3). However, when compared to a sensor made of a common nondegradable piezoelectric PVDF-TrFE film (which exhibits a higher d$_{33}$ of approximately −34 pC/N), the biodegradable 4,000 rpm electrospun PLLA sensor appears to produce lower-amplitude signals under the same applied force (*SI Appendix*, Fig. S10). We also show that the charge output from the same 4,000 rpm sensor is stable for over 10,000 cycles of the same impact force (10 N). Not only is the 4,000 rpm electrospun film more sensitive, but its higher crystallinity does not appear to result in any significant changes to the degradation rate when compared to the bulk PLLA piezoelectric film (*SI Appendix*, Fig. S11). Without being encapsulated, the PLLA films exhibit a reduction in piezoelectricity after being exposed to aqueous environments due to plastic deformation under an applied load (*SI Appendix*, Fig. S12). We then demonstrate the use of the nanofiber sensor to monitor intraabdominal pressure in a mouse. The sensor (5 × 5 mm) is fully implanted into the abdominal cavity of a mouse and connected to a small printed circuit board (PCB) via a subcutaneous (s.c.) biodegradable wire made of Mo and coated in PLLA (*SI Appendix, Methods*). The PCB contains a charge amplifying circuit, a wireless near-field communication (NFC) chip and a commercial antenna (*SI Appendix, Methods*). The entire PCB is sealed inside an 18 × 14-mm PDMS (polydimethylsiloxane) box and s.c. implanted at the back of the animal (Fig. 4*C*). Thus, the abdominal sensor and the connecting wires can self-degrade, while the nondegradable PCB could be easily removed at the end of the sensor's lifetime in a minimally invasive manner. The mouse's abdomen, filled with saline solution, is then manually stimulated to generate an internal fluid pressure, which mimics a change in intraabdominal pressure (*SI Appendix, Methods*). A clearly distinguishable signal (Fig. 4*D*) is wirelessly measured while the mouse's abdomen is periodically depressed and relaxed. The measured pressure signal was then compared to the signal generated by a 300 rpm PLLA sensor (negative control) to verify the signal was not generated by triboelectricity and motion artifacts of the wires (Fig. 4*D*). These results clearly demonstrate the potential of the biodegradable PLLA sensor for monitoring vital physiological pressures inside the body.

In addition to monitoring intraabdominal pressure, we demonstrate that the same PLLA nanofiber sensor can also be used as a biodegradable US transducer. We first tested the PLLA nanofibers' ability to transmit or receive ultrasonic waves. During US transmission testing (Fig. 5 *A*, *Inset*), a capsule hydrophone was used to measure the acoustic pressure. The PLLA device was driven by a function generator to produce a continuous ultrasonic wave at 1 MHz (*SI Appendix, Methods*). As seen in Fig. 5*A*, there was no signal detected when the function generator is "off." When the generator was "on," all PLLA transducers generated distinct acoustic waves while the 300 rpm sample (negative-control sample, nonpiezoelectric) resulted in only noise (*SI Appendix*, Fig. S13). The trend is similar in the US receiving test, as illustrated in *SI Appendix*, Fig. S14; in all of these experiments, the highly aligned 4,000 rpm sample provided the highest conversion signals. Interestingly, the PLLA transducers can act as speakers to generate audible sounds and even play music (Movies S1–S3). We also conducted a degradation experiment and demonstrated that a transducer, using encapsulating layers of untreated PLLA (100 μm thick), can have a lifetime of up to 8 d in phosphate buffer saline (PBS) at 37 °C (Fig. 5*B*) (*SI Appendix, Methods*). Longer functional lifetimes can certainly be achieved by engineering the properties [i.e., thickness or molecular weight (MW)] of the encapsulating PLLA layers (3) or using other biodegradable encapsulating polymers.
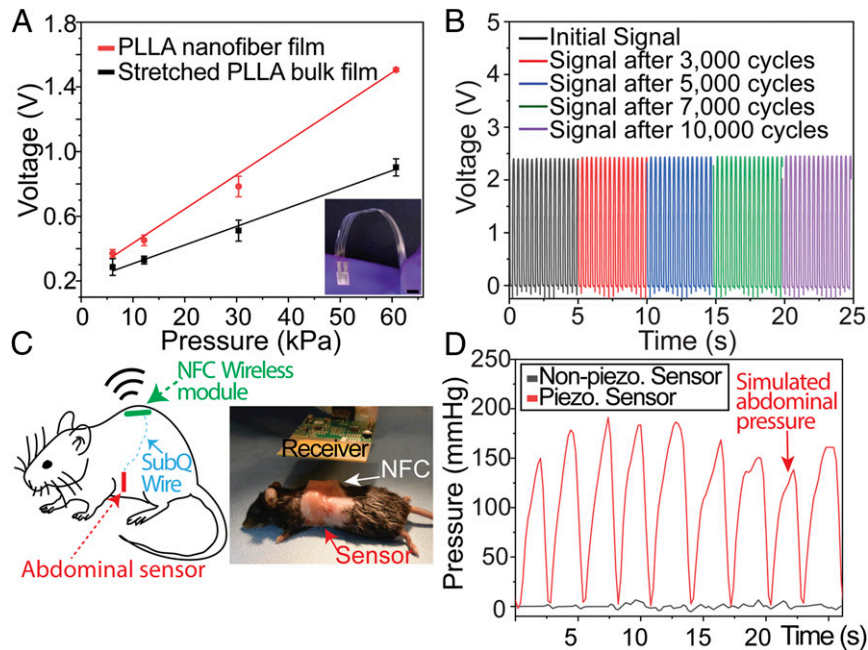
Curry et al.

Fig. 4. Wireless, biodegradable PLLA-nanofiber force sensor. (*A*) Comparison of calibration curves for a biodegradable sensor using stretched, bulk piezo-PLLA film (black) and a 4,000 rpm electrospun PLLA nanofiber film (red). *Inset* shows the optical image of the biodegradable and flexible force sensor, made from the PLLA nanofibers. (Scale bar, 5 mm.) (*B*) Output from a charge amplifying circuit connected to a 4,000 rpm electrospun, biodegradable PLLA sensor that is subjected to 10,000 cycles of a 10-N force. (*C*) Simplified schematic of the implanted, wireless pressure sensor in a mouse (*Left*) and optical image of a mouse receiving the wireless PLLA sensor implanted (*Right*). NFC, near-field communication chip. (*D*) Comparison of the simulated abdominal pressure signals, wirelessly recorded from an implanted biodegradable PLLA nanofiber sensor using a 300 rpm negative control (black) and a 4,000 rpm film (red).

Importantly, for a proof-of-concept on a potential application of the biodegradable transducer, we employ the PLLA device, made of 4,000 rpm nanofiber samples, for disruption of the BBB in vivo. The experiment is illustrated in Fig. 6*A*. A 5 mm × 5 mm biodegradable US transducer, which is connected to flexible, biodegradable PLLA-encapsulated Mo wires, was placed on a craniotomy defect in a mouse skull (*SI Appendix, Methods*). The spatial pressure field of the biodegradable transducer is provided in *SI Appendix,* Fig. S15. The transducer was operated at 1 MHz to generate an acoustic pressure of 0.3 MPa (rarefaction pressure value) in a series of 2 shots lasting 30 s, with a 30-s break between each shot (*SI Appendix,* Fig. S16). The device functioned well in its predefined lifetime and eventually self-degraded (Fig. 6*B*). We processed the brains for fluorescence analysis of bloodborne elements to gauge leakage of the BBB (*SI Appendix, Methods*). Two indicators of leakage were intentionally chosen in order to reflect the relative degree of BBB disruption. Tissue autofluorescence at 488 nm is associated with the presence of the 64.5 kDa (in MW) blood protein hemoglobin (39, 40), which has been suggested to leak across a disrupted BBB (41). As seen in Fig. 6*C*, a noticeable halo of autofluorescence (green stain) could be seen around various microvessels (red stain) in the brains of mice sonicated by the 4,000 rpm transducer. In contrast, no similar signal was observed from the same coronal sections (C2) of the control mouse, sonicated by the 300 rpm nonpiezoelectric control sample. Additional brain sections of the control mouse (receiving the nonpiezoelectric device) are provided in *SI Appendix,* Fig. S17. As further illustrated in Fig. 6*D* and *SI Appendix,* Fig. S18, for the mice that received US treatment, the closer the coronal sections are to the implanted transducer, the more disrupted vessels are associated with autofluorescent signals. This serves as an internal control and clearly shows the local US-induced BBB opening. The BBB opening was again confirmed by immunofluorescence analysis on the leakage of the serum protein IgG (~150 kDa) (*SI Appendix,* Fig. S19). To further certify the potential application of the

biodegradable device for delivering drugs through the BBB, another in vivo animal model was performed. The procedure of this experiment is similar to the previous experiment except that the dextran (3 kDa, FITC, Lysine Fixable; Thermo Fisher) as a drug model was retro-orbitally injected into the mice after the sonication process (*SI Appendix, Methods* and Fig. S20). Additionally, another control group in which mice did not receive the microbubbles before sonication was added to this experiment in order to validate the effect of microbubbles in the BBB opening. As seen in Fig. 6 *E, Left*, a remarkable level of green signal (FITC) was found around the microvessels in the brain of mice that received the treatments by the 4,000 rpm transducer and microbubbles. It is noticeable that the intensity of the FITC signal is reduced at deeper areas of the brain. On the other hand, no green signal was detected from the same
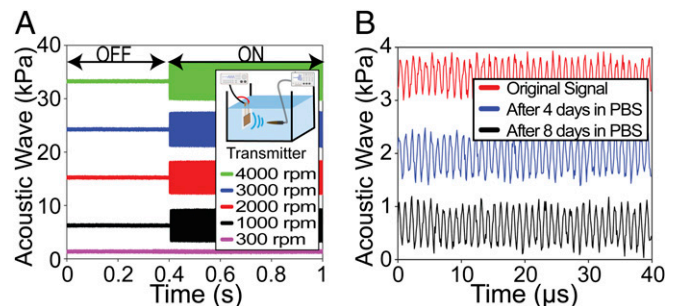

Fig. 5. US characterization of the biodegradable PLLA-nanofiber transducer. (*A*) The output pressure from the transducer with different electrospinning speeds under the same input voltage. The *Inset* is the simplified schematic of the experiment. (*B*) Output pressure from a biodegradable US transducer made from 4,000 rpm electrospun PLLA under the same input voltage after different days in PBS at 37 °C.
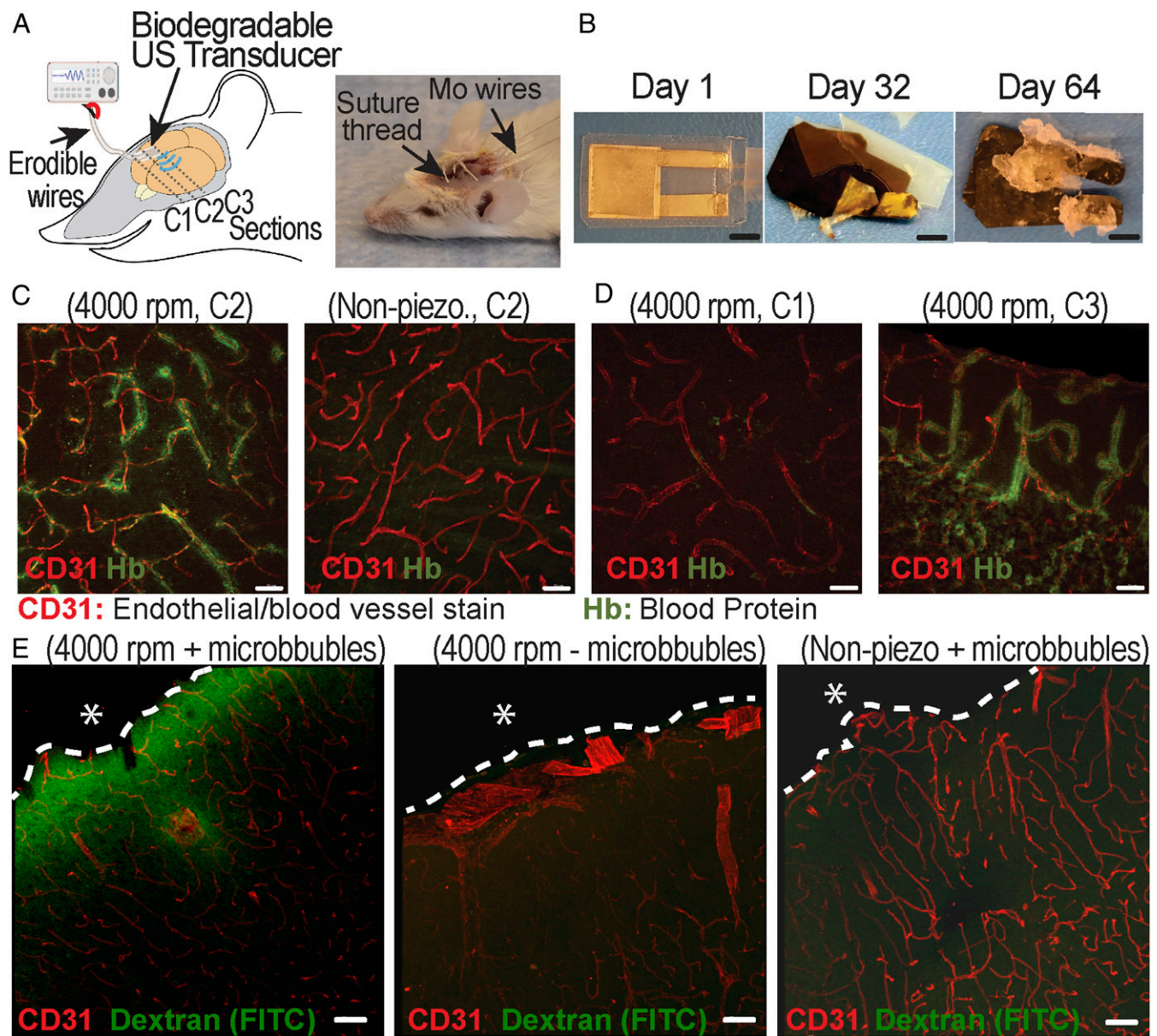
Fig. 6. In vivo experiment to demonstrate the application of PLLA nanofiber transducer for the BBB opening and drug delivering. (*A*) The schematic (*Left*) and optical image (*Right*) of the in vivo experiment. (*B*) The optical images of a typical biodegradable US transducer at different days in the buffered solution at an accelerated-degradation temperature of 70 °C. (Scale bars, 5 mm.) (*C*) Representative images showing the autofluorescent signal of blood protein at the coronal section (C2) from the brains of mice that received US from the 4,000 rpm PLLA transducer (*Left*) and the 300 rpm PLLA negative-control transducer (*Right*). (*D*) Representative images show the blood protein signal at different coronal sections of the same mouse brain receiving the US treatment. Section C3 (*Right*) is closer to the implanted transducer, while section C1 (*Left*) is far away from the implanted US transducer, serving as an internal control. (Scale bars in *C* and *D*, 30 μm.) (*E*) Representative images show the signal of dextran (FITC) at the coronal sections from the brains of mice that received different treatments and samples. The dashed lines show the boundary between the brain and the biodegradable device. The asterisk (*) shows the position of the implanted device. (Scale bars, 50 μm.)

coronal sections of the two control samples, Fig. 6 *E*, *Center* and *Right*. Additional representative images of the brain sections in the experimental group, as well as the control groups, are provided in *SI Appendix*, Figs. S21 and S22. If higher output acoustic pressure and wireless powering are needed for the US transducer, we can fabricate the device with multiple layers of PLLA nanofiber films and utilize the inductive coupling effect, as demonstrated in *SI Appendix*, Figs. S23–S25, and *SI Appendix*, Figs. S26 and S27, respectively.

Finally, to demonstrate the biocompatibility of the PLLA nanofiber devices, we implanted these devices s.c. into the backs of mice and the intracranial cavity of rats (*SI Appendix, Methods*) for histology analysis. The histological images from both experiments showed that the device elicits minimal fibrosis and immune response after implantation for 2 and 4 wk, as seen in *SI Appendix*, Figs. S28–S30. Collectively, these results illustrate that the biodegradable PLLA transducer can be implanted safely into the brain to locally and effectively open the BBB, which could facilitate the delivery of drugs into the brain for the treatment of various brain diseases or disorders. Built upon materials commonly utilized in medical implants, the transducer can self-degrade, causing no harm to the body, and avoid any invasive brain surgery for removal.

Curry et al.

www.manaraa.com

Conclusions

We have presented a strategy for materials processing, device assembly, electronic integration, and piezoelectric stimulation to 1) create biodegradable piezoelectric PLLA nanofibers with stable, effective, and highly controllable piezoelectric performance, and 2) demonstrate implanted-device applications of this powerful nanomaterial, including a biodegradable, wireless, highly sensitive pressure sensor and a biodegradable ultrasonic transducer. All of these piezoelectric implants employ only common biodegradable and biocompatible materials that can safely self-degrade, avoiding undesired invasive removal surgeries. In future applications, these piezoelectric devices could be used to harvest energy from normal body motions, thereby eliminating the need for batteries often required by conventional medical implants. The PLLA nanofibers could also serve as a tissue scaffold that can generate electrical stimulation under body motions to promote tissue regeneration. We therefore anticipate the PLLA nanofibers, and the biodegradable piezoelectric devices described herein can profoundly impact various fields of medicine, ranging from tissue engineering and drug delivery to medical implanted sensors/transducers/actuators.

Materials and Methods

Details of fabrications and characterizations of the PLLA nanofiber films, the force sensor, and the US transducer along with in vitro and in vivo experiments all appear in *SI Appendix*. Animal procedures are approved and performed following Institutional Animal Care and Use Committee guidelines at the University of Connecticut and University of Connecticut Health Center.

Data Availability Statement. All data supporting the findings of this study are available within the article and/or its supplementary materials.

1. M. T. Chorsi *et al.*, Piezoelectric biomaterials for sensors and actuators. *Adv. Mater.* **31**, e1802084 (2019).
2. T. D. Nguyen *et al.*, Piezoelectric nanoribbons for monitoring cellular deformations. *Nat. Nanotechnol.* **7**, 587–593 (2012).
3. E. J. Curry *et al.*, Biodegradable piezoelectric force sensor. *Proc. Natl. Acad. Sci. U.S.A.* **115**, 909–914 (2018).
4. Y. Ikada, Y. Shikinami, Y. Hara, M. Tagawa, E. Fukada, Enhancement of bone formation by drawn poly(ʟ-lactide). *J. Biomed. Mater. Res.* **30**, 553–558 (1996).
5. Y. Tajitsu, M. Kanesaki, M. Tsukiji, K. Imoto, M. Date, E. Fukada, Novel tweezers for biological cells using piezoelectric polylactic acid fibers. *Ferroelectrics* **320**, 133–139 (2005).
6. Q. Cui, C. Liu, X. F. Zha, Study on a piezoelectric micropump for the controlled drug delivery system. *Microfluid. Nanofluidics* **3**, 377–390 (2007).
7. C. Li, P.-M. Wu, L. A. Shutter, R. K. Narayan, Dual-mode operation of flexible piezoelectric polymer diaphragm for intracranial pressure measurement. *Appl. Phys. Lett.* **96**, 053502 (2010).
8. C. Dagdeviren *et al.*, Conformable amplified lead zirconate titanate sensors with enhanced piezoelectric response for cutaneous pressure monitoring. *Nat. Commun.* **5**, 4496 (2014).
9. R. Woltjer *et al.*, (2016) "Optimization of piezo-MEMS layout for a bladder monitor" in *2016 IEEE International Ultrasonics Symposium (IUS)* (IEEE, 2016), pp. 1–4.
10. A. Idbaih *et al.*, Safety and feasibility of repeated and transient blood–brain barrier disruption by pulsed ultrasound in patients with recurrent glioblastoma. *Clin. Cancer Res.* **25**, 3793–3801 (2019).
11. N. McDannold, N. Vykhodtseva, S. Raymond, F. A. Jolesz, K. Hynynen, MRI-guided targeted blood-brain barrier disruption with focused ultrasound: Histological findings in rabbits. *Ultrasound Med. Biol.* **31**, 1527–1537 (2005).
12. M. Kinoshita, N. McDannold, F. A. Jolesz, K. Hynynen, Noninvasive localized delivery of Herceptin to the mouse brain by MRI-guided focused ultrasound-induced blood-brain barrier disruption. *Proc. Natl. Acad. Sci. U.S.A.* **103**, 11719–11723 (2006).
13. N. Vykhodtseva, N. McDannold, K. Hynynen, Progress and problems in the application of focused ultrasound for blood-brain barrier disruption. *Ultrasonics* **48**, 279–296 (2008).
14. J. O. Szablowski, A. Lee-Gosselin, B. Lue, D. Malounda, M. G. Shapiro, Acoustically targeted chemogenetics for the non-invasive control of neural circuits. *Nat. Biomed. Eng.* **2**, 475–484 (2018).
15. C. Horodyckid *et al.*, Safe long-term repeated disruption of the blood-brain barrier using an implantable ultrasound device: A multiparametric study in a primate model. *J. Neurosurg.* **126**, 1351–1361 (2017).
16. D. da Silva *et al.*, Biocompatibility, biodegradation and excretion of polylactic acid (PLA) in medical implants and theranostic systems. *Chem. Eng. J.* **340**, 9–14 (2018).
17. S. Lee *et al.*, Lactic acid assisted fabrication of bioactive three-dimensional PLLA/β-TCP fibrous scaffold for biomedical application. *Chem. Eng. J.* **347**, 771–781 (2018).
18. S. Farah, D. G. Anderson, R. Langer, Physical and mechanical properties of PLA, and their functions in widespread applications—a comprehensive review. *Adv. Drug Deliv. Rev.* **107**, 367–392 (2016).
19. Y. Tajitsu, Fundamental study on improvement of piezoelectricity of poly(ʟ-lactic acid) and its application to film actuators. *IEEE Trans. Ultrason. Ferroelectr. Freq. Control* **60**, 1625–1629 (2013).
20. M. Ando *et al.*, Pressure-sensitive touch panel based on piezoelectric poly (l-lactic acid) film. *Jpn. J. Appl. Phys.* **52**, 09KD17 (2013).
21. M. Ando *et al.*, "New human machine interface devices using a piezoelectric poly(ʟ-lactic acid) film" in *2013 IEEE International Symposium on the Applications of Ferroelectric and Workshop on the Piezoresponse Force Microscopy (ISAF/PFM)* (IEEE, 2013), pp. 236–239.
22. S. Guerin *et al.*, Control of piezoelectricity in amino acids by supramolecular packing. *Nat. Mater.* **17**, 180–186 (2018).
23. G. Zhao *et al.*, Electrospun poly(ʟ-lactic acid) nanofibers for nanogenerator and diagnostic sensor applications. *Macromol. Mater. Eng.* **302**, 1600476 (2017).
24. A. Sultana *et al.*, Human skin interactive self-powered wearable piezoelectric bio-e-skin by electrospun poly-ʟ-lactic acid nanofibers for non-invasive physiological signal monitoring. *J. Mater. Chem. B* **5**, 7352–7359 (2017).
25. S. J. Lee, A. P. Arun, K. J. Kim, Piezoelectric properties of electrospun poly(ʟ-lactic acid) nanofiber web. *Mater. Lett.* **148**, 58–62 (2015).
26. C. M. Boutry *et al.*, Biodegradable and flexible arterial-pulse sensor for the wireless monitoring of blood flow. *Nat. Biomed. Eng.* **3**, 47–57 (2019).
27. C. M. Boutry *et al.*, A stretchable and biodegradable strain and pressure sensor for orthopaedic application. *Nat. Electron.* **1**, 314–321 (2018).
28. C. M. Boutry *et al.*, A sensitive and biodegradable pressure sensor array for cardiovascular monitoring. *Adv. Mater.* **27**, 6954–6961 (2015).
29. J. K. Chang *et al.*, Biodegradable electronic systems in 3D, heterogeneously integrated formats. *Adv. Mater.* **30**, 1704955 (2018).
30. S.-K. Kang *et al.*, Bioresorbable silicon electronic sensors for the brain. *Nature* **530**, 71–76 (2016).
31. M. Yoshida, T. Onogi, K. Onishi, Y. Inagaki, Y. Tajitsu, High piezoelectric performance of poly (lactic acid) film manufactured by solid-state extrusion. *Jpn. J. Appl. Phys.* **53**, 09PC02 (2014).
32. M. Smith, Y. Calahorra, Q. Jing, S. Kar-Narayan, Direct observation of shear piezoelectricity in poly-ʟ-lactic acid nanowires. *APL Mater.* **5**, 074105 (2017).
33. J.-F. Ru *et al.*, Dominant β-form of poly(ʟ-lactic acid) obtained directly from melt under shear and pressure fields. *Macromolecules* **49**, 3826–3837 (2016).
34. V. Sencadas *et al.*, Local piezoelectric activity of single poly(ʟ-lactic acid) (PLLA) microfibers. *Appl. Phys. A* **109**, 51–55 (2012).
35. T. Wartzek, T. Lammersen, B. Eilebrecht, M. Walter, S. Leonhardt, Triboelectricity in capacitive biopotential measurements. *IEEE Trans. Biomed. Eng.* **58**, 1268–1277 (2011).
36. H. H. Peltoniemi, D. Hallikainen, T. Toivonen, P. Helevirta, T. Waris, SR-PLLA and SR-PGA miniscrews: Biodegradation and tissue reactions in the calvarium and dura mater. *J. Craniomaxillofac. Surg.* **27**, 42–50 (1999).
37. J. A. Novotny, J. R. Turnlund, Molybdenum intake influences molybdenum kinetics in men. *J. Nutr.* **137**, 37–42 (2007).
38. W.-C. Witzleb, J. Ziegler, F. Krummenauer, V. Neumeister, K.-P. Guenther, Exposure to chromium, cobalt and molybdenum from metal-on-metal total hip replacement and hip resurfacing arthroplasty. *Acta Orthop.* **77**, 697–705 (2006).
39. C. G. Atkins, K. Buckley, M. W. Blades, R. F. B. Turner, Raman spectroscopy of blood and blood components. *Appl. Spectrosc.* **71**, 767–793 (2017).
40. T. Kobayashi, K. Nakata, I. Yajima, M. Kato, H. J. B. Tsurui, Label-free imaging of melanoma with confocal photothermal microscopy: Differentiation between malignant and benign tissue. *Bioeng.* **5**, 67 (2018).
41. A. Lewin *et al.*, Free serum haemoglobin is associated with brain atrophy in secondary progressive multiple sclerosis. *Wellcome Open Res.* **1**, 10 (2016).

www.manaraa.com